sensors MDPI

Article

Extended joint sparsity reconstruction for spatial and temporal ERT imaging

Bo Chen [1], Juan F.P.J. Abascal [2] and Manuchehr Soleimani [1,*]

[1] Engineering Tomography Lab (ETL), Department of Electronic and Electrical Engineering, University of Bath, BA2 7AY Bath, UK; B.Chen@bath.ac.uk
[2] Univ Lyon, INSA-Lyon, Université Claude Bernard Lyon 1, UJM-Saint Etienne, CNRS, Inserm, CREATIS UMR 5220, U1206 Lyon, France; juanabascal78@googlemail.com
* Correspondence: m.soleimani@bath.ac.uk

Received: date; Accepted: date; Published: date

Abstract: Electrical resistance tomography (ERT) is an imaging technique to recover the conductivity distribution with boundary measurements via attached electrodes. Wide range of applications has been made using ERT for image reconstruction or parameter calculation due to it is being high speed data collection, low cost, and also have advantage of non-invasive and portable. Although ERT is considered as high temporal resolution method a temporally regularized method can greatly enhance such a temporal resolution compared to frame-by-frame reconstruction. In some of the cases, especially in the industrial applications, dynamical movement of an object is critical. In practice, it is desirable to monitoring and controlling the dynamical process. ERT could find out the spatial conductivity distribution based on lots of previous works, and ERT would potential show good performance on exploiting temporal information as well. Many ERT algorithms reconstructs images frame by frame, which is not optimal and would assuming that the target is static during collection of each data frame, which is inconsistent with the real case. A spatiotemporal based algorithms can account for the temporal effect of dynamical movement and can generate better result, however, there were not so many work aiming at analyzing the performance in time domain. In this paper, we discuss the performance of a novel spatiotemporal total variation (STTV) algorithm on both spatial and temporal domain, and also a Temporal One-Step Tikhonov based algorithms were also employed for comparison. The experimental results show that the STTV would have a faster response time on temporal variation of the moving object. This robust time response can contribute to a much better control process which is a main aim of new generation of process tomography systems.

Keywords: electrical resistance tomography; total variation (TV) algorithm; dynamical ERT

1. Introduction

Electrical resistance tomography has been investigated for few decades since it has been proposed in 1984 as an approach of vivo image reconstruction to obtain the spatial distribution of resistivity of a tissue [1]. Many applications has benefited from ERT technique due to its advantages of being low cost, high speed and non-invasive. The implementation of ERT requires a conductive domain where electrodes required to be directly attached on its boundary. Electric field is generated from injecting the current via electrodes pattern where Alternating Current (AC) source would be required. For voltage measurement, volt meters would be applied to electrodes simultaneously. The measurement strategy could be selected among neighboring method, opposite method, adaptive method, etc. [2]. A typical ERT problems would normally begin with forward problem, where distribution of the potential could be worked out using simulation modeling tool. The sensitivity distribution of the whole domain could be calculated via perturbation method [3]. Then, the conductivity distribution could be recovered via inverse problem solver, which is known as algorithm to reconstruct images from measured real boundary data.

The inverse problem of electrical tomography are actually ill-posed, and regularization methods, in this case, would be very important for recovery of conductivity mapping. Methods using strategy of least square solution, such as, Tikhonov regularization, was quite popular. However, it would give a result with blurred edge of the object boundary, and lead to reconstruction error due to Tikhonov would over smoothed the images. In the past many years, another method called total variation (TV) with different TV functional, such as, [4, 5] has been proposed. TV triggered many attention, as higher-qualitied images could be obtained.

According to dynamical ERT cases, most of the traditional ERT algorithms reconstructs static images using individual frames of data which assuming that no correlations between adjacent frames, such as, Tikhonov [6], Gauss-Newton one-step [7], and total variation [8] etc. However, to reconstruct images with the regularization methods that working frame by frame may not be an optimal choice, ~~as high~~and would result in overlapping artefacts images, although only a few of papers had proposed methods that account for temporal correlation effect. High temporal resolution is one of the advantage of ERT system, and information of the correlation between individual frames ~~might~~is worth to be explored to contribute to the image quality. There were few ~~methods tracking the moving object~~ types of algorithms that ~~using~~account for the ~~spatiotemporal information~~temporal correlation effects. First of all, Kalman filtering has been used in different tomographic techniques. For example, ~~in 1998,~~ M. Vauhkonen firstly proposed Kalman filter method (1998) to track fast changes in electrical impedance tomography (EIT) [9]. ~~Following that, P. J. Vauhkonen and M. Vauhkonen evaluated the~~More recent works regarding Kalman filter ~~and smoother approach, and compared it with traditional algorithms using phantom experiments data [10]. In [11], M.~~ in dynamical imaging field are also proposed, for example, M. Soleimani and M. Vauhkonen [10] were using Kalman filter on electrical capacitance tomography (ECT) and electromagnetic induction tomography (EMT), and demonstrated Kalman filtering approach could improve the spatiotemporal resolution~~.~~ (2007). A. Lehikoinen et al (2009) evaluates dynamical conductivity distribution in porous medium using Extended Kalman Filter [11]. A. K. Saibaba (2014) tracked CO_2 movement with a fast Extended Kalman Filter [12]. In addition, another algorithm known as temporal one-step solver (TOS), which is based on GN one-step method has been proposed by A. Adler and T. Dai (2007) in [~~12~~13], and has been investigated by comparing with ~~other approaches, such as,~~ Kalman filter and conventional GN one-step method~~. A 4D regularization was proposed afterwards,~~ which ~~combined both spatial (3D)~~are working as if no correlations between successive frames. More recently, Yerworth and ~~temporal priori,~~Bayford (2013) first proposed interpolating EIT measurements for propose of according with the fact that conductivity is changing during acquisition of frame [14]. Gagnon, Hervé, et al (2015) proposed comparison works to assess to advantages and drawbacks of previous presented approaches using different types of data frames with three reconstruction algorithms [15]. Chen, Bo, et al (2018) proposed a novel spatiotemporal total variation (STTV) method for assessing the performance of 2D and 3D moving objects using both simulation ~~method based on EIDORS [13~~and experimental results [16]. Temporally linked algorithms such as the one shown in above examples are providing an opportunity for faster data collection and less averaging in ERT data. A smooth ~~temporal~~ regularization ~~how where~~however will limit the time resolution. A temporal TV with TV regularization in time can overcome this problem, providing both high speed and sharp temporal responses.

In practice, ERT could potentially be combined with a tomography-based control system. To reach the requirement of controlling application, high-quality images from ERT would be needed, and useful information are supposed to be extracted based on these reconstructed results for the proposes of, for example, implementation of emergency operation to avoid undesirable condition. In this paper, we particularly interested in the temporal and spatial performance of spatiotemporal total variation (STTV) method~~ that has been proposed in [14].~~. By comparing it with TOS algorithm, ~~which has been used in [12],~~ we want to explore spatiotemporal information along the time domain~~.~~, and assess the gradients and time response of both approaches. The results of this paper are based on 2D phantom experimental tests with ~~static and~~ dynamical movement of inclusion. For each set of the results, STTV and TOS are employed using the same measured data set to ensure the consistence.

2. Method

ERT is reconstructed images based on its boundary measurement data. Regarding a common ERT model, the conductive domain is normally bounded by electrodes, where the electric field generated from injected currents. The participation of inclusion would change the distribution of electric field, which would affect the boundary measurement data, and hence, conductivity distribution images would be affected. In terms of one injection between a pair of electrodes, the electric field is produced, and the generated voltage between other electrodes pairs could be measured and recorded via ERT system as measured data. For a 16-electrode ring, there will be 208 individual measurement data for both background and object, where a set of 208 corresponding voltage difference $\Delta\boldsymbol{u}$ will be used as boundary data to reconstruct a frame of image. In this paper, we are testing the performance of dynamic cases. The difference between the static and dynamic case is that the object keep moving its position, which makes the electric field keep changing the distribution at the same time, where the effects of magnetic fields is not considered in order to simplify this physical model. Due to the process of current injection as well as the conductive field are remained, both cases would have the same forward model. However, the time step of data collection cannot be neglected in practical dynamic case as the dynamic electric field would affect the data measurement although this could be very fast.

2.1. Forward Problem

For a specific region of ERT, forward problem is to estimate the potential distribution based on the given applied current on electrodes, shape of the region, and a known conductivity. The forward solver are mainly using finite element method (FEM), which discrete the domain into many elements, then we can work out the potentials distribution from the values on the nodes between elements using simulation tool. In this paper, the condition is under low excitation frequency, which created the assumption for the physical model that the effect of magnetic induction could be neglected for such a pure resistive model in a quasi-static electric field. For an ERT domain Ω with its boundary $d\Omega$, the current density is contributed by conductive current J_C and the conductive current density J_s which should remain at 0 since no source of the internal domain, the governing formulation ~~(1)~~ could be derived from ~~Maxwell's equation [15~~following equations [17]

$$\cancel{\nabla\cdot\sigma\nabla\varphi}\nabla\times E = 0$$

$$\nabla\cdot J = 0$$

$$J = \sigma E$$

$$E = -\nabla\varphi \tag{1}$$

Where σ is conductivity, and $-E, \varphi$ donates electric field and electric potential~~, which also have~~. The first three equations are given by charge conservation law, Faraday's law and continuum version of Ohm's law respectively. With low frequency assumption in Maxwell's equations ignoring the ~~expression with electric field E:~~ wave propagation effects, the ERT forward problem can be described by:

$$\cancel{E = -\nabla\varphi} \quad \nabla\cdot\sigma\nabla\varphi = 0 \tag{2}$$

The current density j is generated while the current injected sequentially via electrodes on the boundary of the domain, in this case, boundary condition must be involved. With $\vec{n}$ representing normal vector which gives:

$$\cancel{j}$$

$$j = \sigma\frac{\partial\varphi}{\partial\vec{n}} \tag{3}$$

Regarding the electrode model, a complete electrode model (CEM), which combined the features from other previous models [~~16~~18] was chose and have the following formulations:

$$u + z_l.\sigma\frac{\partial u}{\partial \vec{n}} = v_l \qquad \cancel{(4)}(4)$$

~~$\sum_{n=1}^{N} I_n = 0$~~ On the boundary, the current and voltage Kirchhoff laws must be satisfied:

$$\oiint_{d\Omega} j \cdot dS = 0 \qquad (5)$$

$$\cancel{\sum_{n=1}^{N} V_n = 0} \quad \oint E \cdot dl = 0 \qquad (6)$$

In the equation (4), the expression displayed the relationship of boundary potential v_l, the potential u on the electrode and the voltage drop on the contact impedance z_l on each electrode. Note that the current density remains 0 on the gap (between electrodes). In order to get unique solution, equation (5) and (6) are involved here, which represents the conservation of charge and the voltage. Both equation could also be simplified as sum of current/potential on all electrodes, which are also equals to zero.

To simplify the ~~problem~~expression, a forward operator could be defined:

$$F(\sigma) = u \qquad (7)$$

A simplified equation could also be given by:

$$\Delta u = \cancel{J}\boldsymbol{J} \cdot \Delta\sigma + \cancel{n}\, noise \qquad (8)$$

Where $\boldsymbol{J}$ donates Jacobian matrix, and defined as $\frac{\delta u}{\delta \sigma}$~~, and n could represent the noise.~~.

2.2. Inverse Problem

The Inverse problem of ERT is actually to obtain the conductivity distribution and get images reconstructed, which requires the inversion of the formulation (8). However, the equation is actually non-linear, and the inverse problem of ERT is ill-posed, which means the existence, uniqueness, and the stability of the solution are not meet at the same time [~~17~~19]. In this case, regularization methods are required for the optimization problem.

In the static ERT, the electrical conductivity can be described by $\sigma(x, y, z)$, whist a time-varying conductivity in dynamical ERT means that the conductivity can be described by $\sigma(x, y, z, t)$. In the actual ERT experiments, we are dealing with the discrete number of spatial and time steps, which can be described by spatial and time resolutions. In dynamical ERT, with moving inclusions, the assumptions of forward modeling equation (2) is still valid, and conductivity is changing from $\sigma(x, y, z)$ to $\sigma(x, y, z, t)$. Further extension of static inversion to a temporal inversion is described in the following section.

In this paper, we are discussing the cases about dynamical 2D ERT reconstruction. In this case, the expected conductivity difference would be a 3D object, which contains both spatial and temporal components. Comparison between Spatiotemporal Total Variation Algorithm (STTV) and Temporal one-step solver (TOS) will be made. Some results are displayed and discussed in section 3 and 4.

2.2.1. Spatiotemporal Total Variation Algorithm

The Spatiotemporal Total Variation Algorithm is based on Split Bergman method, and has been used to reconstruct the images from a flow system in [~~14~~16]. For solving an inverse problem, a penalty term could be added for optimization. The penalty term of a total variation problem are normally given by $G_{TV} = \alpha\|\nabla\Delta\sigma\|_1$. STTV combined spatial and temporal TV functional, and the constrained problem of STTV is given by (9), and formulations (10) and (11) represent its iterative scheme:

$$arg\min_{\Delta\sigma}\left\|\nabla_{x,y}\Delta\sigma\right\|_1 + \|\nabla_t\Delta\sigma\|_1 \quad \text{s.t.} \quad \left\|\tilde{J}\Delta\sigma - \Delta u\right\|_2^2 \le \delta \qquad (9)$$

$$\Delta\sigma^{k+1} = arg\min_{\Delta\sigma}\left\|\nabla_{x,y}\Delta\sigma\right\|_1 + \|\nabla_t\Delta\sigma\|_1 + \sum_{i=1}^{I}\frac{\mu}{2}\left\|\tilde{J}\Delta\sigma - \Delta u^k\right\|_2^2 \qquad (10)$$

$$\Delta u^{k+1} = \Delta u^k - \tilde{J}\Delta\sigma^{k+1} + \Delta u, \qquad (11)$$

Due to the difficulty of solving an non-differential TV functional, auxiliary variables dx,dx,dt are involved here for applying the ‘splitting’, which is a similar with Split Bregman that splitting the data fidelity term and the non-differentiable l1-norm penalty term. Spatiotemporal component is included in STTV to correlate the consecutive frames, rather than recover $\Delta\sigma$ individually. As

$$(\Delta\sigma^{k+1}, dx, \mathrm{dy}, dt) = arg \min_{\Delta\sigma, dx, \mathrm{dy}, \mathrm{dt}} \|(dx, \mathrm{dy})\|_1 + \|dt\|_1 + \frac{\mu}{2}\left\|\tilde{\mathrm{J}}\Delta\sigma - \Delta\mathrm{u}^k\right\|_2^2 \ \mathrm{s.t.} \quad \mathrm{d}_i = \nabla_i \Delta\sigma, \mathrm{i} = \mathrm{x}, \mathrm{y}, \mathrm{t} \quad (12)$$

2.2.2. Temporal One-Step Solver

Another algorithm called temporal one-step solver (TOS) was proposed in [~~12~~13] in 2007, which was based on Gauss-Newton one-step algorithm. Instead of reconstruct images frame by frame, TOS is using a data set that combined with the data of nearby frames of frame n, where the data set and the conductivity change could be given by:

$$\widetilde{\Delta u_n} = [\Delta u_{n-d}, \cdots, \Delta u_n, \ldots, \Delta u_{n+d}]^T \quad (13)$$

$$\widetilde{\Delta\sigma_n} = [\Delta\sigma_{n-d}, \cdots, \Delta\sigma_n, \ldots, \Delta\sigma_{n+d}]^T \quad (14)$$

Where in (13) and (14), it takes d frames of data before and after frame n, in this case, the length of the data set would be (2d+1), and d is an integer and must be smaller than n.

The forward problem could be modified into:

$$\widetilde{\Delta u_n} = \tilde{J}\widetilde{\Delta\sigma_n} + noise \quad (15)$$

Using GN One-step method, the inverse problem would be defined as:

$$\left\|\widetilde{\Delta u_n} - \tilde{J}\Delta\sigma_n\right\|^2 + \lambda^2\left\|\widetilde{\Delta\sigma_n}\right\|^2 \quad (16)$$

By solving (16), as stated in [12], the formulation is written as:

$$\widetilde{\Delta\sigma_n} = [gamma \otimes (PJ^T)][gamma \otimes (JPJ^T) + \lambda^2(I \otimes V)]^{-1} \cdot \widetilde{\Delta u_n} \quad (17)$$

In (17), V is an identical matrix, and equals to R^{-1} , where $R = \alpha R_1 + \beta R_2 + \gamma R_3$. R_1 is contribute to a NOSER prior , a diagonal matrix with its diagonal elements equivalent with the diagonal elements of $J \cdot J^T$. R_2 donates an identical matrix with the size of R_1.

3. Experiments and Results

3.1. Experimental Setting up

Data collection of experiments in this paper would require a complete ERT system, which composed with an ERT Hardware system, PC (with software) and a sensor.

The hardware system has been used in this paper is known as EIT Swisstom Pioneer system [~~18~~20] with 32 channels, which has following main components:

- 16 double-channel EIT chips to control 32 electrode
- Smart SensorBeltConnector that integrated with AC current injection (1-7mA, 50KHz-250KHz), voltage signal demodulating, high speed data collection (up to 80 frames/second)
- Interface module: Frame synchronisation input and output, synchronisation signal, power management between SensorBelt and SensorBeltConnector
- Power supply

The STEM data collection software is running with the Swisstom EIT Pioneer to collect data, where the excitation frequency, current peak value, data collection speed and current pattern are available to be adjusted. In addition, the connection with electrode could easily be checked via Sensor Quality panel, and real-time dynamical image is also available.

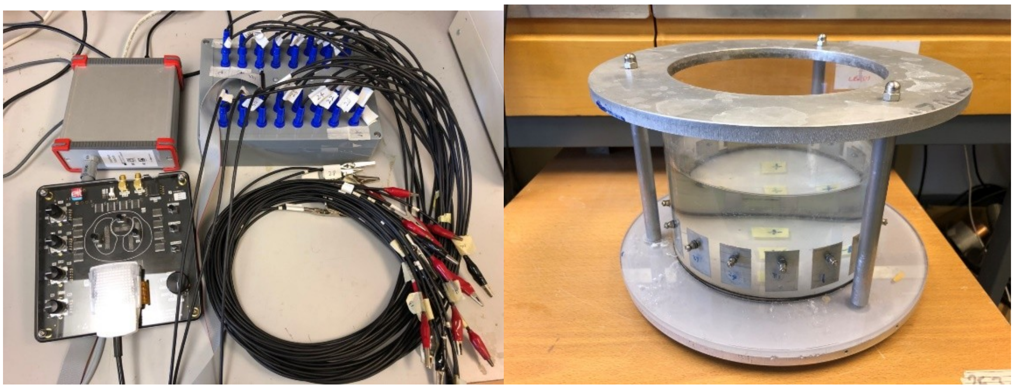

(a) (b)

Figure 1: (a) Swisstom EIT Pioneer system (b) experimental tank.

- Sensor

The 2D sensor has been used in experiments is a cylinder-shape PMMA container, with diameter of 19cm and height of 25 cm. On the side wall of the sensor, 16 electrodes (2cm x 4cm) are evenly fixed along the surface. A heavy circular metal board is sitting on the top of the container, connected by three long screws with the base board, in order to avoid leaking of any liquid.

3.2. Experimental Tests

In this section, we are showing reconstructed images of different tests. Tap water and a plastic bar (3.1 cm diameter) were used as background and the moving object under tested respectively. Cross movement and circular movement were considered as two types of movement in the dynamical test. In all of the experimental tests, the peak value of exciting current has been used is 7mA, and operation frequency is 270 KHz. To well compare two algorithms, lots of data has been collected under various data collection rate on various dynamic cases for image reconstruction. In this section, we only displayed some typical results here in each part. Different dynamical movement type has been setting up, and results from each type of dynamical movement using both algorithms are displayed. Regarding the image reconstruction, there are 6 images are extracted from the generated dynamical image of each movement type to demonstrate the performance of both algorithms.

Dynamical Test

Dynamical test is divided by two types of movement in this paper: cross movement and circular movement. Cross movement is the case that the inclusion moving cross the domain through the center along the diameter from one side to the other, and the circular movement is the type of the movement that the object moving along a circle near the boundary of the domain. The illustration of the dynamical movement can be seen in the figure below.

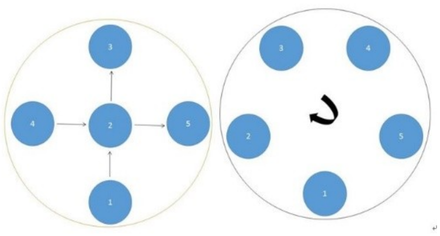

(a) **(b)**

Figure 2: Illustration of the dynamical movement type. The cross movement is showing in (a), and (b) illustrates the circular movement.

Test 1 Cross Movement

In the first dynamical test, it was setting up that the plastic bar was driving manually to move from bottom to the top, then from left to right cross the domain respectively. As showing in the figure 2 (a), the inclusion movement cross the domain from 1 to 3 via the position 2 in the centre, then it move from 4 to 5. The excitation current was using 7mA with frequency of 270 KHz, and the data collection rate has been used is 24 frames/second. On both tests of the cross movement, 850 and 950 frames of measurement data has been collected with background data included. The measurement data that taken from the background (with tap water only) is more than 100 frames when we keep more than 5 seconds before we start to put the plastic bar into the tank, so the average background data of the first hundred frames would be used for the propose of removing some noise. By using STTV and TOS algorithms respectively, reconstructed images are produced, as displaying in the Table below, where the second column of the Table showing the images of TOS algorithm, and results from STTV are placed in third column. There are 6 slices of images has been included in the Table to demonstrate the recovery images of the movement process using both algorithms.

No.	TOS	STTV
1	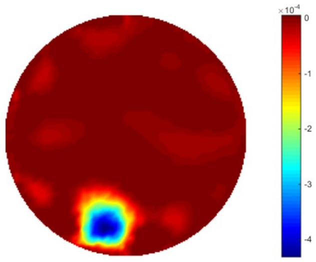	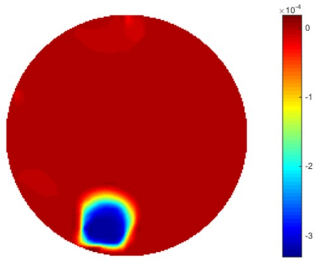
2	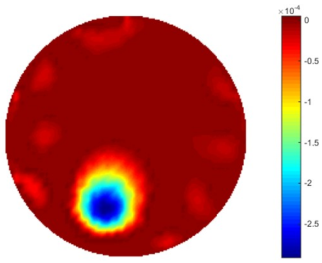	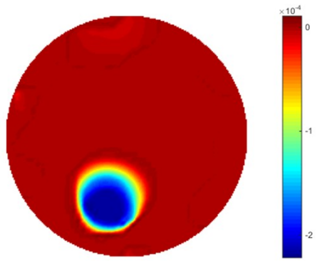
3	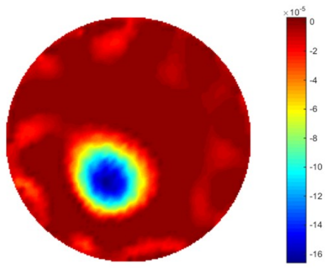	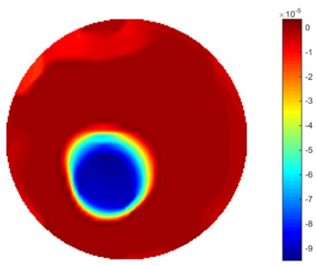
4	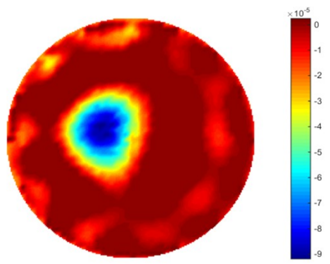	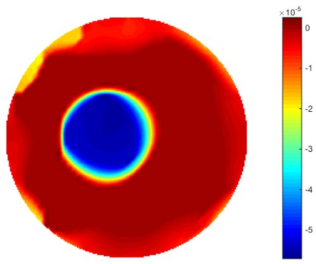

5	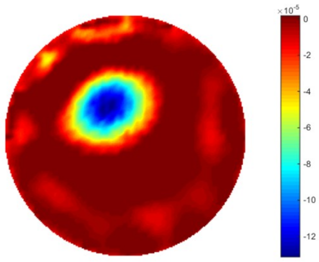	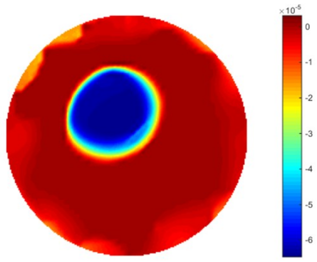
6	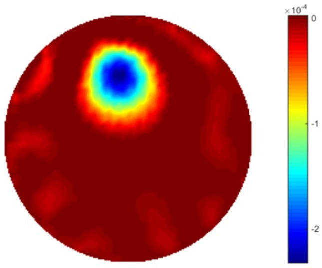	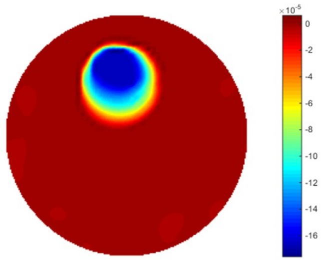

Table 1: Reconstructed images of cross movement in Test 1, where the inclusion is moving from the bottom to the top.

No.	TOS	STTV
1	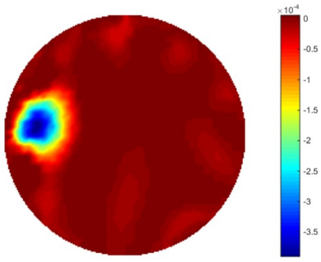	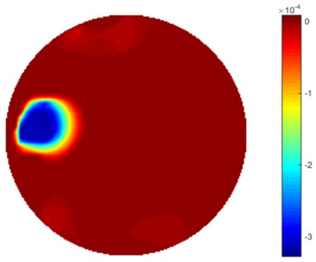
2	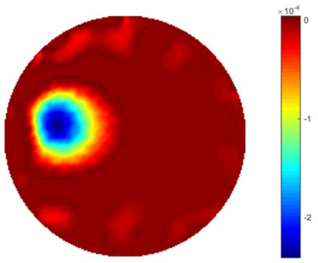	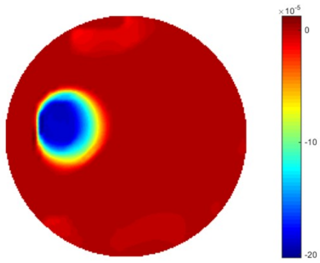
3	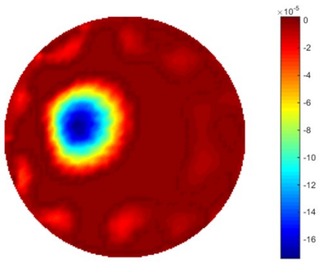	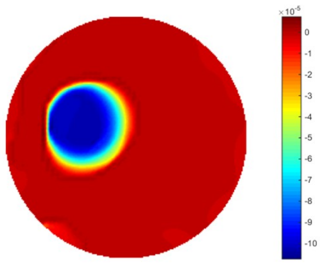

4	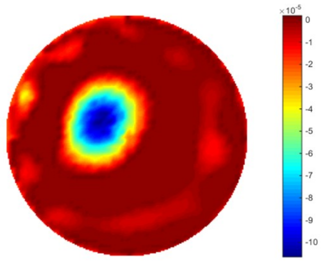	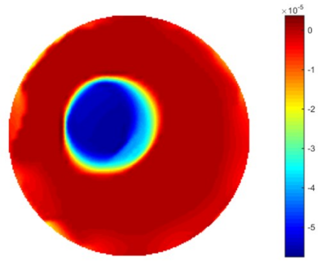
5	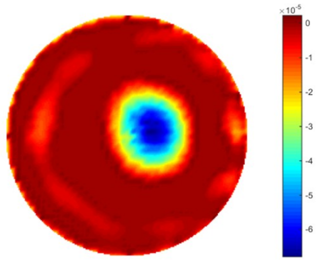	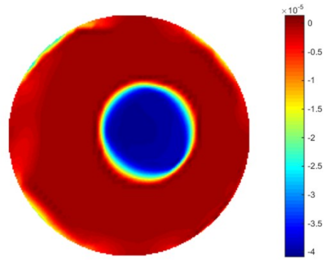
6	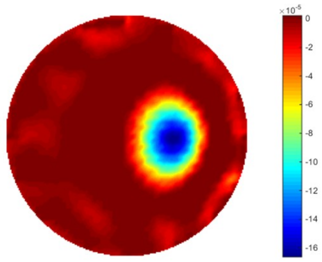	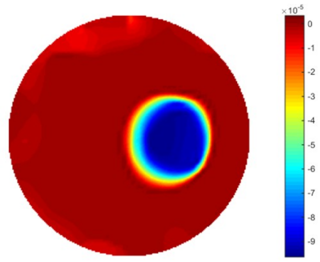

Table 2: Reconstructed images of cross movement in Test 1, where the inclusion is moving from left hand side to the right hand side

From the results that displayed on both Tables, it could be found that the moving process is monitored successfully and kept consistent with the movment of the plastic bar within the tank. Regarding the quality of reconstructed images, images from using STTV have sharp object boundary and very smooth inside the object or on the background area, while the other ones have blurred object edge. In terms of the performance of the temporal domain, many previous work using the methods to produce dynamical images with individual frames of data. However, what can be seen from the Table is the object is keeping consistent on its shape with both algorithms without any streching along the movment direction.

Test 2 Circular Movement

The implementation of the circular movement is similar with the Test 1, where same excitation current value, frequency are employed. Data collection speed of 50 frames/second has been used for the boundary data measurement. The bar was moving clockwise along the circle that close to the boundary and start with the location at the bottom that showing in figure 2 (b). There are 530 frames of boundary collected with about 150 frames of background data. In terms of the implementation of using STTV algorithm, it worth to point out that we need to make sure that the background data is not included. For example, if the first 10 or 20 frames are still the data of background, more noise would be added in, which would introduce useless information and degrade the image quality, as STTV using the time gradient to correlates each frames. Reconstructed images from STTV and TOS are compared in the Table below.

The reconstructed images in this type of movement are quite stable compare with the result from cross movement test. From these pictures, STTV still shows a better sharpness and a more smooth background than TOS.

No.	**TOS**	**STTV**
1	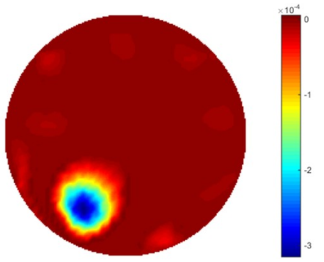	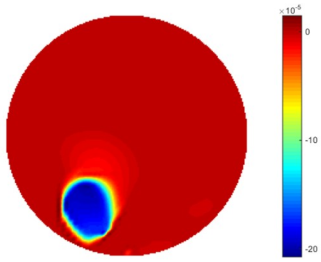
2	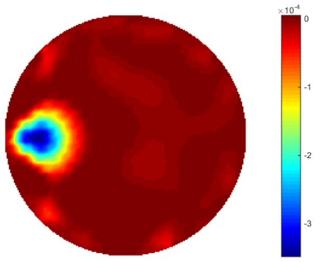	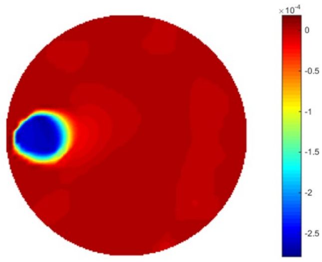
3	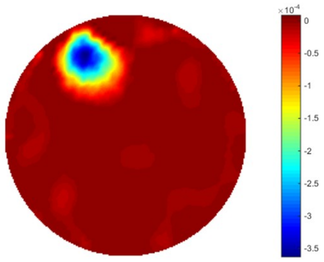	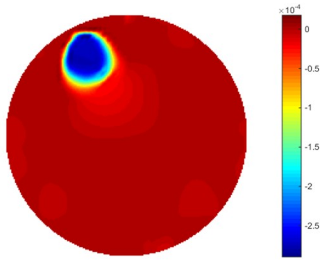
4	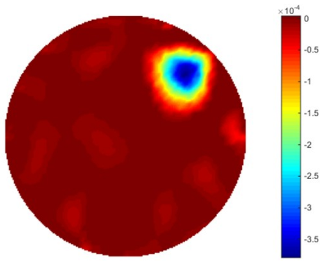	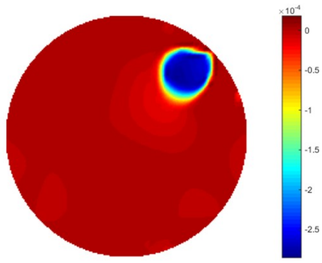
5	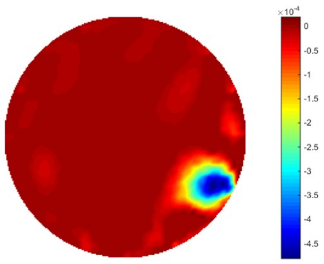	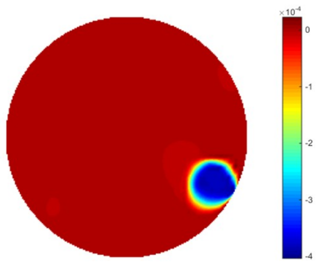

6		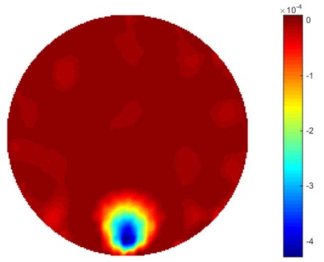	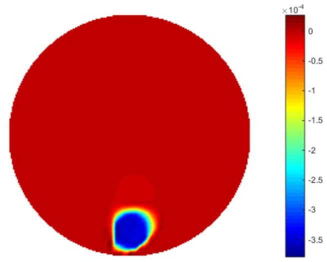

Table 3: Reconstructed images from circular movement test.

In conclusion, both algorithms shows good performance on dynamical test regarding the images. In comparison, images reconstructed using STTV indicates better quality due to its sharpness and less noisy. However, the discussions in this chapter are based on images only. To further support the good performance of STTV, some parameters about exploiting spatial and temporal information will be calculated, and some quantitative analysis based on these calculation will be carried out.

4. Analysis and Discussion

As what has been shown in the last chapter, images generated from TOS algorithm are slightly suffering from blurred boundary of recovered object, but STTV could produce higher-quality images, as those image benefit from its sharpness and less noisy. To analyze the advantages and drawback of both algorithms, in this section, some quantitative information would be extracted and displayed to compare two algorithms. The analysis would based on calculated results of gradient, where spatial and temporal gradients are discussed separately. The response time are defined and work out for both methods in order to further demonstrate how both algorithms contribute to the performance on time domain.

4.1. Definition of Gradients and Time Response

a. Spatial Gradient

The spatial gradient of an image means how the conductivity is changing in space, which would normally be calculated along a direction (x, or y). The x/y-gradient could also be understood as the change of the slope value of the spatial distribution along x/y direction. For image u, the gradient of x and y direction could be calculated by:

$$\nabla_x u = \frac{\Delta u}{\Delta x} \qquad (S/m) \tag{18}$$

$$\nabla_y u = \frac{\Delta u}{\Delta y} \qquad (S/m) \tag{19}$$

Where $\nabla_x u$ and $\nabla_y u$ are spatial gradient of x and y direction, and Δu is the conductivity step-change between 2 pixels. u is a slice of image with 51 by 51 pixels, and $p = 51$. In this paper, the magnitude of the gradient was calculated, which is given by:

$$\nabla_{xy} u = \sqrt{(\nabla_x u)^2 + (\nabla_y u)^2} \tag{20}$$

B. Temporal Gradient

Temporal imaging is defined as dynamical image reconstructions along the time series. Time gradient is useful for determining the dynamical performance as it describe the step changes of the whole variation process. The time gradient of dynamical image could also be explained as the variation of the variations of conductivity in a pixel in time domain. The dynamical process of the object could react to the temporal change in pixel values.

If we extract pixel values along time sequence, the conductivity change on this pixel would be plotted as a 1-D line graph, where the pixel value variation could illustrates the circumstance of the object movement. The temporal gradient could be defined as how much variation has been made on each time step with the time sequence, which is also a discrete gradient as data set is combined with individual frames of data, although they are time correlated. The gradient on time could be calculated by:

$$\nabla_t u = \frac{\Delta u}{\Delta t} \qquad \left(\frac{S}{m}/s\right) \tag{21}$$

C. Time Response

Time Response is defined by how fast it is capable of reacting to temporal change, which could be used to determine the dynamical performance of the result quantitatively. Regarding the temporal change in a pixel that the inclusion has experienced during the moving process, the algorithm that shows faster response would be an optimal choice. The expression of Time Response could be given by a time interval that corresponds to where the conductivity decay from the background value to the peak value.

4.2. Spatial and Temporal Gradients

A. Spatial Imaging

In the Tables 4-6, there are few items are displaying here: images of spatial gradient, 1-D plots of spatial distribution and the corresponding plots of the spatial gradient. There are 3 Tables in this part, where 3 slices are extracted for the analysis.

For an ideal case, the boundary of the object is supposed to be clear, so the spatial distribution on the object boundary is expected to be sharp, and the whole object area and also the background should be remained at its corresponding conductivity values. A 1-D Plot of Spatial distribution of a perfect ideal case would show a square-shape wave, which results that only two sharp changes would be seen between the object and background. Some comparisons has been made between STTV and TOS algorithms, as displayed in the Tables 4-6.

From the images of the spatial gradient on three different positions (the data has been used in this part are consistent with the tests in last chapter) within the tank, regarding the results using TOS, the object area is unevenly distributed in the images of spatial gradient distribution, however the results from STTV are showing very clear object boundary. The comparison of the conductivity distribution is given by the 1-D plot in the third row of each table, where images has been normalized in order to making contrast. The blue and red colored line in the plotted line graphs are indicating the result that recovered from STTV and TOS respectively about spatial distribution and gradient changes. It could be seen from the conductivity distribution using TOS that the lowest value are always in the middle of the wave, and it is dropping down gradually and come back up slowly again, which indicates unclear boundary between the background and the object, as it would be hard to recognize where exactly corresponds to the boundary. The plots from STTV are given by nearly square-shape waves. The plotted line is always keeping flat either in the background or the object area, and a very shape change is observed between the background and the target. The last graph is showing the comparison of the spatial gradient, in which the plots of STTV always display two sharp change which has the same wave shape of the plot from true image, but the gradient plot of TOS result are deforming due to its less sharpness of the recovered target.

Algorithm	TOS	STTV
Spatial gradient (S/m)	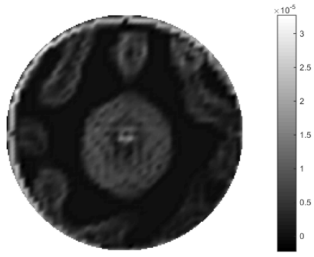	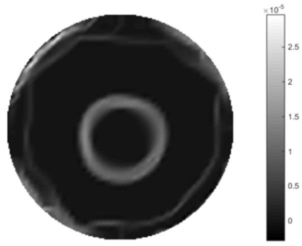
1-d plot of spatial distribution	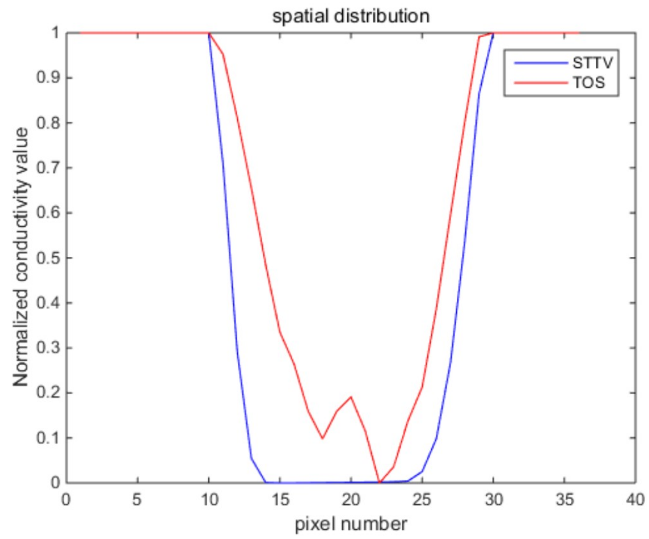	
1-d plot of spatial gradient	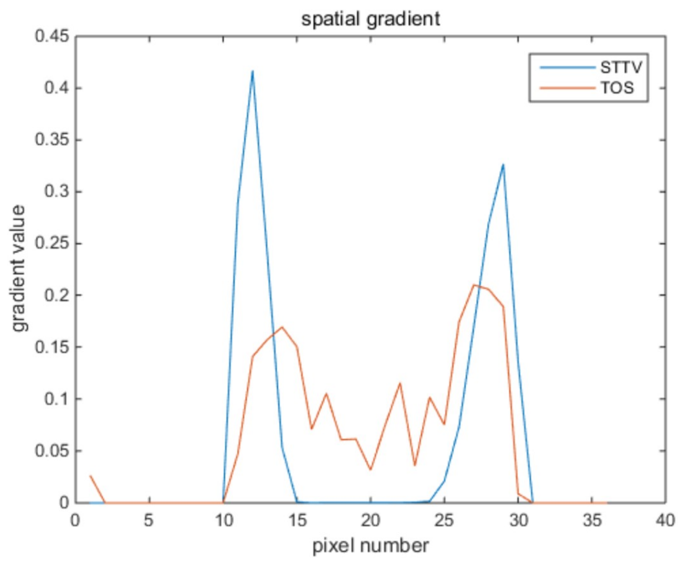	

Table 4: Spatial gradients of the results produced from STTV and TOS algorithms, where the reconstructed object is near the center. The image of the spatial gradient is generated from calculating the gradient of reconstructed image. The spatial distribution plotted in the second row is using the middle row of the image matrix, and the 1-d plot of spatial gradient produced to evaluate the spatial variation.

Algorithm	TOS	STTV
Spatial gradient (S/m)	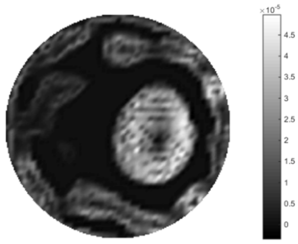	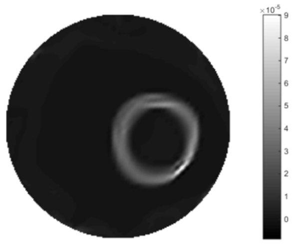
1-d plot of spatial distribution	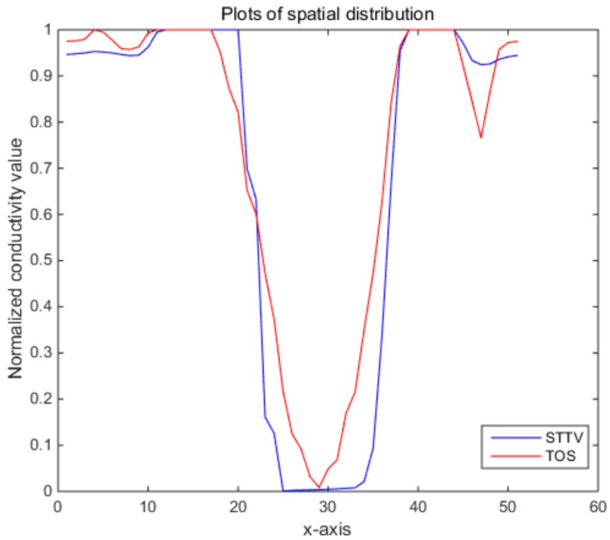	
1-d plot of spatial gradient	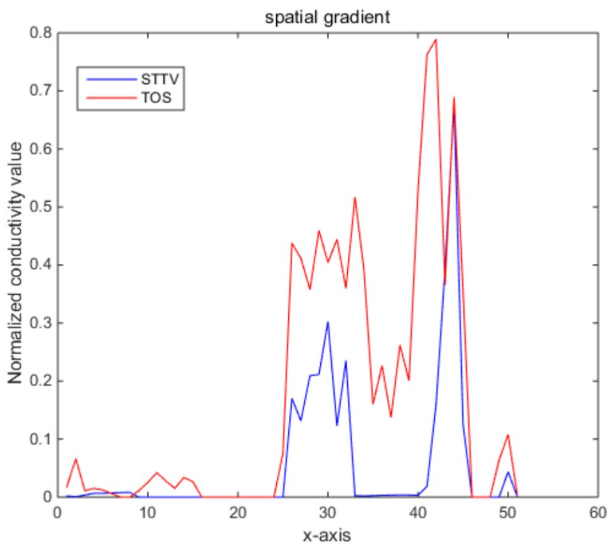	

Table 5: Spatial gradients of the results produced from STTV and TOS algorithms, where the reconstructed object is coming to the second position.

Algorithm	TOS	STTV
Spatial gradient (S/m)	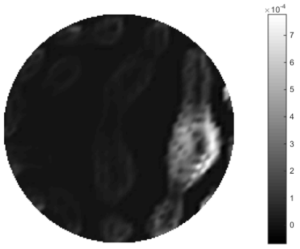	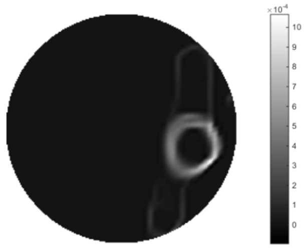
1-d plot of spatial distribution	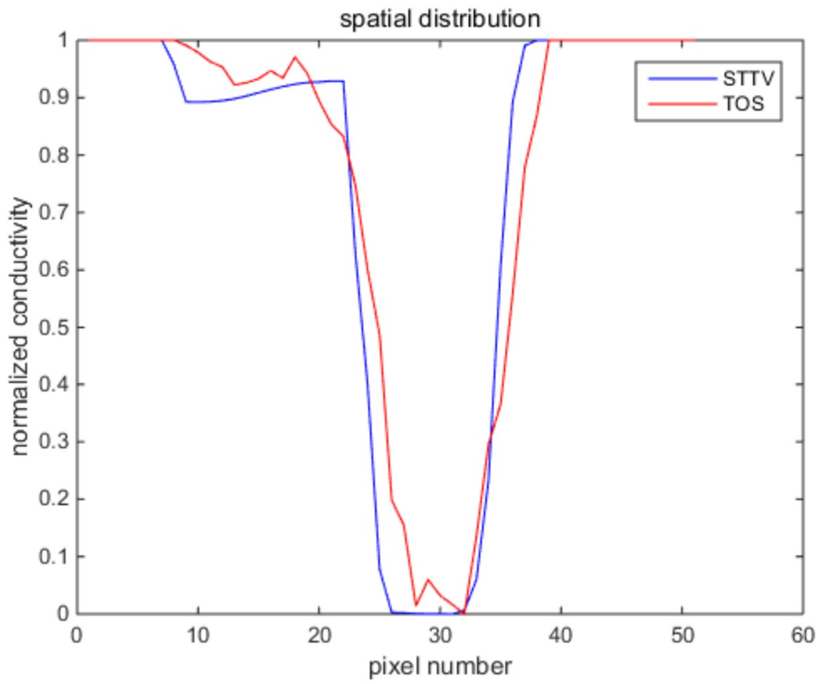	
1-d plot of spatial gradient	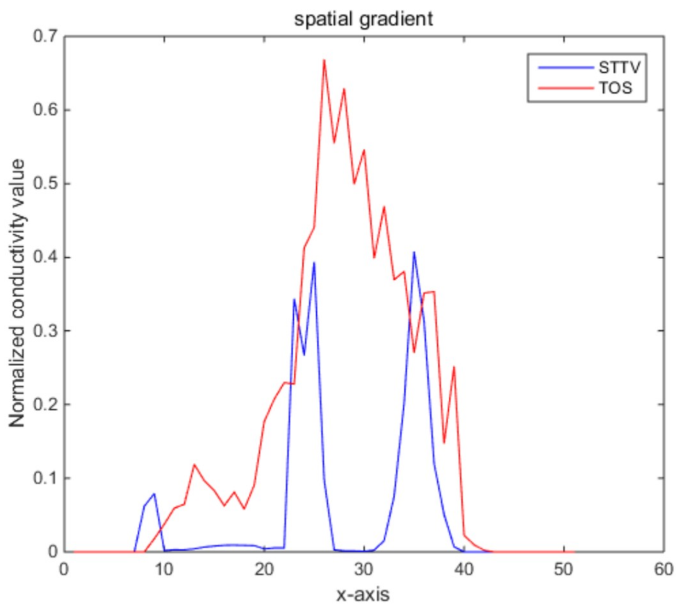	

389 Table 6: Spatial gradients of the results produced from STTV and TOS algorithms, where the
390 reconstructed object is coming to the edge of the domain.

B. Temporal Imaging

Reconstructed results from cross and circular movement tests (images has been shown in the last chapter) using TOS and STTV are displayed in this part for ~~analysing~~analyzing the spatiotemporal performance. First of all, spatial and temporal gradient are displayed and compared. In addition, the temporal variation of both dynamical setting using two different algorithms has been taken into account for discussing about the time response.

In fact, the spatial gradient is the change between the current pixel value and the next neighboring pixel value along the defined direction, whilst the temporal gradient is the variation between two adjacent frames (variation along the time series). The images of gradients in this section is based on a random frame N during the dynamical process, so the spatial gradient would be from the reconstructed image using frame N and the temporal gradient would be the difference between image number N and (N+1). According to the results of gradients, on spatial, obvious change of the conductivity distribution along x, y directions could be observed with clear boundary between the background and inclusion. On the background or inside the object area, the conductivity variation between consecutive pixels is very small as it could be seen that the spatial gradient in these area are tend to 0. By comparing with TOS, results showing that the object is observable and recognizable, however, the conductivity value is keep changing inside the object in both direction, and the less sharpness of the boundary indicates the graduate variation between the background and the inclusion.

Regarding the temporal change between adjacent frames, relatively small variation between consecutive frames should be shown in the temporal domain due to a high data collection speed has been employed. In this case, it would be expected a very little shift on the object boundary, and almost zero change should be detected in the rest of the domain the consecutive frame data should be very similar. As shown in the figures of both dynamical movement type that STTV results are proved that it is more immunity to the noise, and its change in time domain is more consistent compare with the results of TOS. In terms of the decay of the absolute spatial/temporal gradient that based on the gradient images in the second row of the table, the line graph of the result using STTV is showing faster decay than the one using TOS method. The plot of decay is actually displaying extent of the variation from the maximum value to 0, which numerically indicates the performance of spatial and temporal change between neighboring frames. This result is quantitatively demonstrating that STTV would potentially reconstruct high-quality images of dynamical case.

Circular movement

	spatial gradient(S/m)	**temporal gradient**($\frac{S}{m}$/s)
TOS	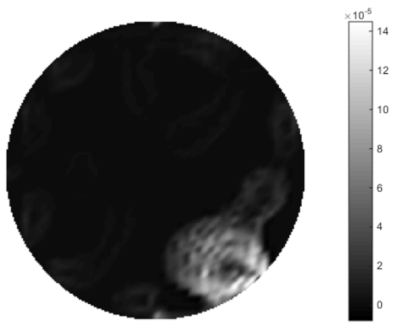	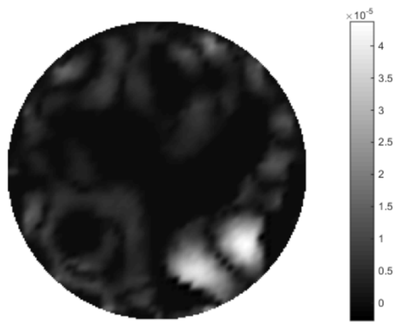

STTV	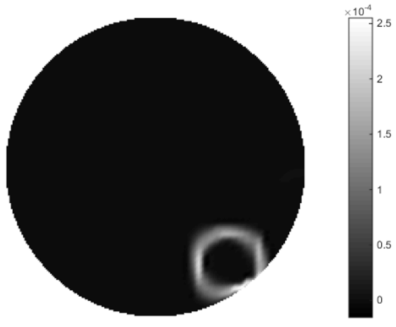	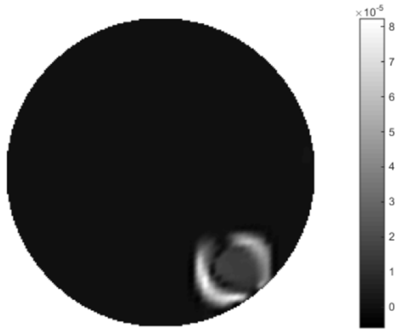
Decay of coefficients in spatial	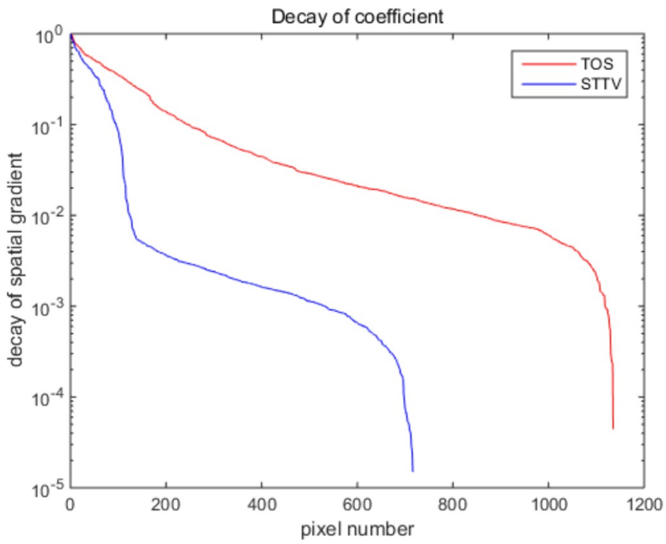	
Decay of coefficients in time	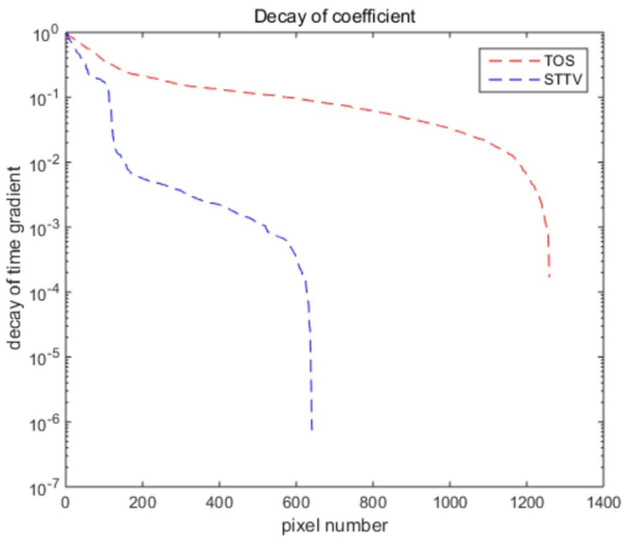	

Table 7: The results of spatial and temporal gradients of circular movement test using STTV and TOS algorithms. The image of the spatial gradient is generated from calculating the spatial gradient of reconstructed image of a specific frame number, and temporal gradient image is based on the time gradient between neighboring frames. The line graph of coefficient decay are based on the gradient value from the images of spatial and temporal gradients

430 **Cross movement**

	spatial gradient(S/m)	**temporal gradient**($\frac{S}{m}$/s)
TOS	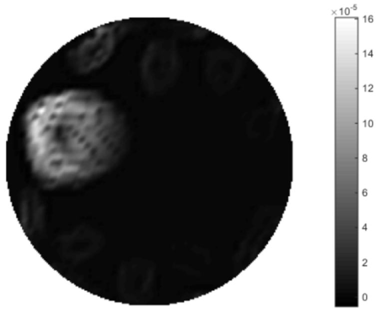	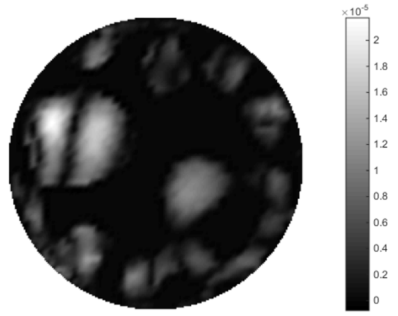
STTV	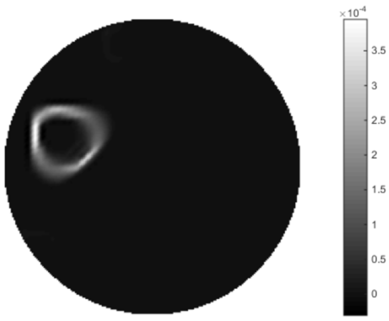	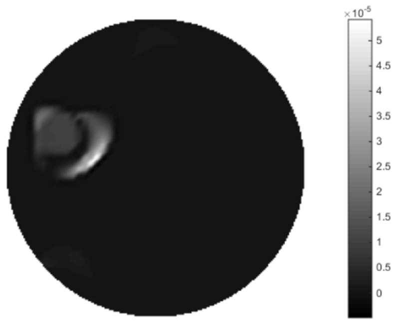
Decay of coefficients in spatial	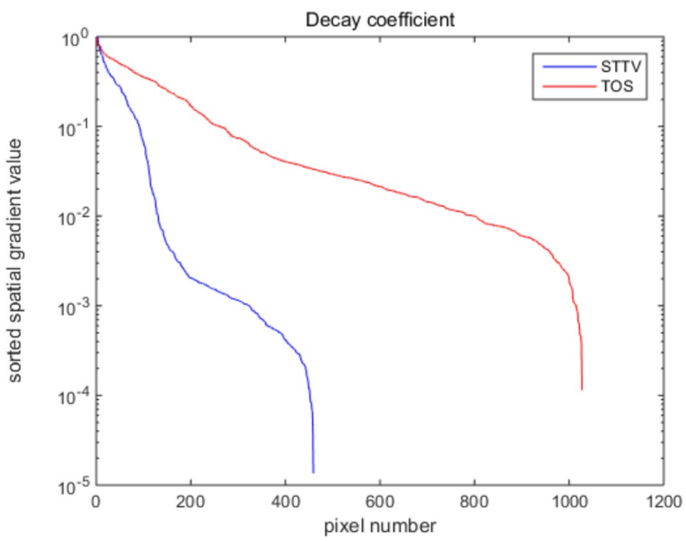	

Decay of coefficients in time	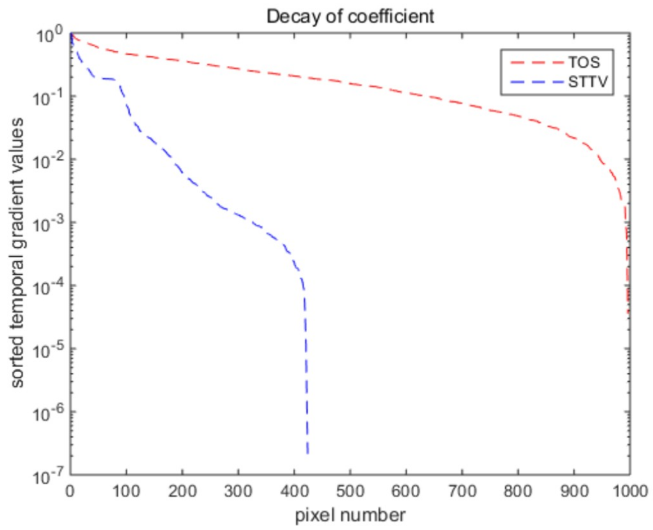

Table 8: The results of spatial and temporal gradients of cross movement test using STTV and TOS algorithms. The image of the spatial gradient is generated from calculating the spatial gradient of reconstructed image of a specific frame number, and temporal gradient image is based on the time gradient between neighboring frames. The line graph of coefficient decay are based on the gradient value from the images of spatial and temporal gradients

4.3. Time Response

To further illustrate the performance in time domain, the conductivity variation on pixels along the time series has been emphasized and taken into further study about the time response. During the dynamical process, when the inclusion come to and then left a pixel, a dynamical change on such pixel would be generated. For a tomography-based control system, it will be quite important that whether an algorithm could well react to a moving inclusion or not, as a timely response is definitely required for making decision and taking implementation in a proper time.

Based on the results from two dynamical movement using both algorithms, conductivity changes along the time series from selected pixels as well as the corresponding temporal gradient are showing in the below two figures. From the time variation plots of both results, it is obviously that they are displaying how fast the conductivity is varying from maximum value (corresponding to the background conductivity) to nearly zero and back up again, where 0 indicates when the object went through the pixel. In comparison, STTV would take slightly shorter to meet its lowest. Numerical calculations of response time of both algorithms are worked out. In the cross movement, the displayed results are from using the data collection speed of 24 frames/second. The response time of both algorithms, in terms of the case that the object entering the pixel, are 2.12s and 3.21s, and in the other movement, the frame speed of 50 frames/second has been used, and STTV shows a time of faster response than TOS. The results stated above indicates STTV got faster response to the conductivity change in time domain.

Cross Movement

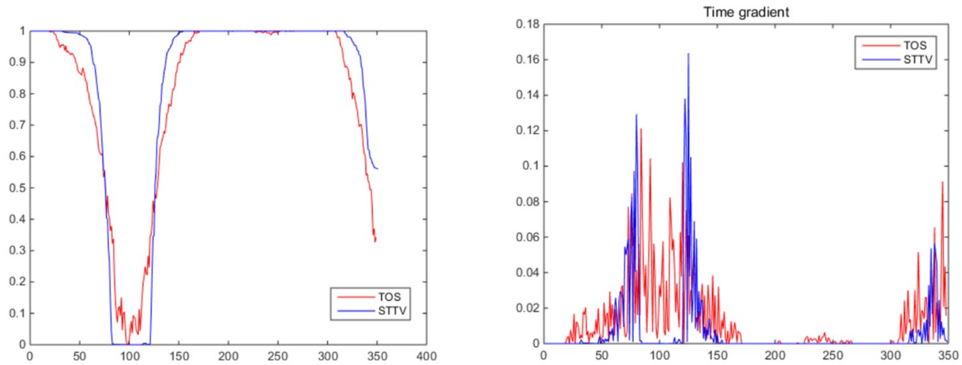

(a) **(b)**

Figure 3: (a) time variation of a pixel extracted from the results of the cross movement (b) the plot of corresponding temporal gradient. The red line stands for the result from using TOS, and the blue line indicates the results of STTV.

Algorithm	~~STTV~~TOS	STTV~~TOS~~
Time response	**~~2.12s (49~~3.21s (77 frames)**	**~~3.21s (77~~2.12s (49 frames)**

Table 9: time response of both algorithms from testing the cross movement

Circular Movement

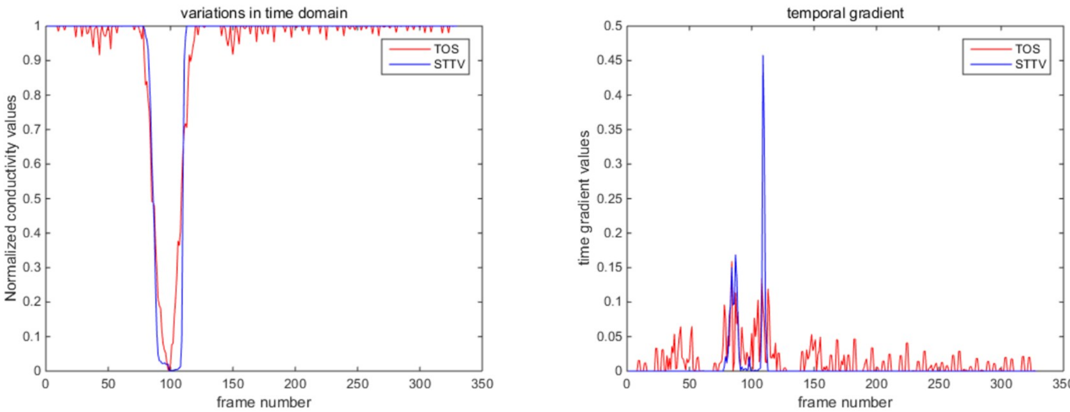

(a) **(b)**

Figure 4: (a) time variation of a pixel extracted from the results of the circular movement (b) the plot of corresponding temporal gradient. The red line stands for the result from using TOS, and the blue line indicates the results of STTV.

Algorithm	TOS~~STTV~~	~~TOS~~STTV
Time response	**0.~~26s (13~~52 s (26 frames)**	**0.~~52 s (26~~26s (13 frames)**

Table 10: time response of both algorithms from testing the circular movement.

5. Conclusion

Dynamical imaging is a very important topic to be investigated due to the fact that there are many requirement regarding moving objects inside the bounded domain in the real life for monitoring and systematic controlling proposes. ERT benefits from its high temporal resolution, and would potentially have temporal information to be exploited along the time domain. In terms of the reconstruction algorithms, the ones using individual frame data are not optimal, as it would ignore the dynamical change and the variation between each time steps could not be considered properly.

In this paper, we are investigating the performance of 2D dynamical movement using experimental data. To evaluate both spatial and temporal performance of STTV algorithm, results from using both STTV and TOS regularization method are displayed for making comparison. In spatial domain, both algorithms shows good performance. Through the analysis on dynamical experiments results, it could be concluded that STTV would generate sharper and less noisy images, However, the optimization of the parameter selection is still required to be studied in the future work, and it would have potential to be upgraded. A sharp image would be preferred as the boundary of recovered images could be detected easier than a blurred one. Performance in time domain of both methods were emphasized compared using temporal gradient and response time, where STTV shows a faster response time on the dynamical change of conductivity based on the quantitative calculation of time response of different dynamical movement. This discovery would be very useful when it will be used in real applications of tomography based control system in the future.

Author Contributions: BC has conducted experimental work and wrote the paper. JFPJ has helped in STTV algorithm. MS has supervised the project and helped with some experimental work. All authors read the paper and commented.

Funding: JFPJ Abascal has received funding from the European Union's Horizon 2020 research and innovation programme under the Marie Sklodowska-Curie grant agreement N° 701915.

Conflicts of Interest: The authors declare no conflict of interest.

References

1. Barber, D C, and B H Brown. "Applied Potential Tomography." Journal of Physics E: Scientific Instruments, vol. 17, no. 9, 1984, pp. 723–733., doi:10.1088/0022-3735/17/9/002.
2. Kauppinen, P., Hyttinen, J. & Malmivuo, J. Sensitivity distribution visualizations of impedance tomography measurement strategies. International Journal of Bioelectromagnetism, 2006, Vol. 8, No. 1, pp. VII/1 - VII/9
3. Brandstatter, B. Jacobian calculation for electrical impedance tomography based on the reciprocity principle. IEEE Trans. Magn. 2003, 39, 1309–1312.
4. X. Song, Y. Xu, F. Dong. '' A spatially adaptive total variation regularization method for electrical resistance tomography'' Meas. Sci. Technol. 26 (2015) 125401 (15pp)
5. Zhou, Zhou, et al. "Comparison of Total Variation Algorithms for Electrical Impedance Tomography." Physiological Measurement, vol. 36, no. 6, 2015, pp. 1193–1209., doi:10.1088/0967-3334/36/6/1193.
6. Vauhkonen, M., et al. "Tikhonov Regularization and Prior Information in Electrical Impedance Tomography." IEEE Transactions on Medical Imaging, vol. 17, no. 2, 1998, pp. 285–293., doi:10.1109/42.700740.

~~7.~~7. Adler A, Guardo R 1996 Electrical impedance tomography: regularized imaging and contrast detection IEEE Trans. Med. Imaging 15 170–179

~~Gagnon, Hervé, et al. "A Comparison Framework for Temporal Image Reconstructions in Electrical Impedance Tomography." Physiological Measurement, vol. 36, no. 6, 2015, pp. 1093–1107., doi:10.1088/0967-3334/36/6/1093.~~

8. Goldstein, T.; Osher, S. The Split Bregman Method for L1-Regularized Problems. SIAM J. Imaging Sci. 2009, 2, 323–343.

9. Vauhkonen, M., et al. "A Kalman Filter Approach to Track Fast Impedance Changes in Electrical Impedance Tomography." IEEE Transactions on Biomedical Engineering, vol. 45, no. 4, 1998, pp. 486–493., doi:10.1109/10.664204.

10. ~~Vauhkonen, P. J., et al. "Dynamic Electrical Impedance Tomography - Phantom Studies." Inverse Problems in Engineering, vol. 8, no. 5, 2000, pp. 495–510., doi:10.1080/174159700088027743.~~

~~11.~~ Soleimani, Manuchehr, et al. "Dynamic Imaging in Electrical Capacitance Tomography and Electromagnetic Induction Tomography Using a Kalman Filter." Measurement Science and Technology, vol. 18, no. 11, 2007, pp. 3287–3294., doi:10.1088/0957-0233/18/11/004.

~~12~~11. A. Lehikoinen, S. Finsterle, A. Voutilainen, M.B. Kowalsky & J.P. Kaipio (2009) Dynamical inversion of geophysical ERT data: state estimation in the vadose zone, Inverse Problems in Science and Engineering, 17:6, 715-736, DOI: 10.1080/17415970802475951

12. A. K. Saibaba, E. L. Miller and P. K. Kitandis, "A fast Kalman filter for time-lapse electrical resistivity tomography," 2014 IEEE Geoscience and Remote Sensing Symposium, Quebec City, QC, 2014, pp. 3152-3155.

13. Adler, A., Dai, T. and Lionheart, W. (2007). Temporal image reconstruction in electrical impedance tomography. Physiological Measurement, 28(7), pp.S1-S11.

~~13. Vauhkonen, M.; Lionheart, W.; Heikkinen, L.; Vauhkonen, P.; Kaipio, J. A MATLAB package for the EIDORS project to reconstruct two-dimensional EIT images. Phys. Meas. 2001, 22, 107–111.~~

~~14.~~14. Yerworth R and Bayford R 2013 The effect of serial data collection on the accuracy of electrical impedance tomography images Physiol. Meas. 34 659–69

15. Gagnon, Hervé, et al. "A Comparison Framework for Temporal Image Reconstructions in Electrical Impedance Tomography." Physiological Measurement, vol. 36, no. 6, 2015, pp. 1093–1107., doi:10.1088/0967-3334/36/6/1093.

16. Chen, Bo, et al. "Electrical Resistance Tomography for Visualization of Moving Objects Using a Spatiotemporal Total Variation Regularization Algorithm." Sensors, vol. 18, no. 6, 2018, p. 1704., doi:10.3390/s18061704.

~~15~~17. Somersalo, Erkki, et al. "Existence and Uniqueness for Electrode Models for Electric Current Computed Tomography." SIAM Journal on Applied Mathematics, vol. 52, no. 4, 1992, pp. 1023–1040., doi:10.1137/0152060.

~~16~~18. Graham, Bradley Michael. "Enhancements in Electrical Impedance Tomography (EIT) Image Reconstruction for 3D Lung Imaging." 2008, pp. 24–25.

~~17~~19. Holder, David S. Electrical Impedance Tomography Methods, History and Applications. Institute of Physics, 2005.

~~18~~20. "EIT Technology." *Swisstom*, Available: www.swisstom.com/en/eit-technology-3.